

# Graph-Theoretic Analysis of Phase Optimization Complexity in Variational Wave Functions for Heisenberg Antiferromagnets

Mahmud Ashraf Shamim,<sup>1,\*</sup> Moshiur Rahman,<sup>2,†</sup> Mohamed Hibat-Allah,<sup>3,4,‡</sup> and Paulo T Araujo<sup>1,§</sup>

<sup>1</sup>*Department of Physics and Astronomy, University of Alabama, Tuscaloosa, 35487, Alabama, USA.*

<sup>2</sup>*Department of Physics, University of Rajshahi, P.O. Box 6205, Rajshahi, Bangladesh.*

<sup>3</sup>*Department of Applied Mathematics, University of Waterloo, Ontario Canada N2L 3G1*

<sup>4</sup>*Vector Institute, Toronto, Ontario, M5G 0C6, Canada*

(Dated: February 6, 2026)

Despite extensive study, the phase structure of the wavefunctions in frustrated Heisenberg antiferromagnets (HAF) is not yet systematically characterized. In this work, we represent the Hilbert space of an HAF as a weighted graph, which we term the Hilbert graph (HG), whose vertices are spin configurations and whose edges are generated by off-diagonal spin-flip terms of the Heisenberg Hamiltonian, with weights set by products of wavefunction amplitudes. Holding the amplitudes fixed and restricting phases to  $\mathbb{Z}_2$  values, the phase-dependent variational energy can be recast as a classical Ising antiferromagnet on the HG, so that phase reconstruction of the ground state reduces to a weighted Max-Cut instance. This shows that phase reconstruction HAF is worst-case NP-hard and provides a direct link between wavefunction sign structure and combinatorial optimization.

**Introduction.** Understanding the physics of geometrically frustrated Heisenberg antiferromagnets (HAF) is among the most challenging problems in modern physics. The difficulty stems from the phase structure of the many-body wavefunction, where frustration generates a complex phase landscape that complicates analytic treatment and precludes a closed-form solution except in a few specialized cases [1–3]. Consequently, progress on the subject has largely relied on variational wavefunction approaches and large-scale numerical simulations [4–6].

Within this variational wavefunction framework, Neural Quantum States (NQS) [7] have emerged as highly expressive ansätze for representing complex many-body wavefunctions in interacting quantum systems. A wide range of NQS architectures have been proposed, yet their practical performance varies significantly across models and regimes. In the case of the HAF, much of this variation can be attributed to whether the model is given an explicit phase prior, such as an imposed sign structure from the Marshall Sign Rule (MSR) [8] to improve accuracy; notable examples include RBMs [7], RNNs [9–11], CNNs [12–15], and SineKANs [16].

This behavior is not universal: hybrid RBM-projected-pair (PP) ansätze [17, 18] and Vision Transformer (ViT)-based NQS [19–22] can achieve competitive accuracy even without an explicit phase prior. These observations indicate that architectural inductive bias can alleviate, but not fundamentally resolve, the difficulties associated with reconstructing the ground-state (GS) phase structure.

Despite their universal approximation capabilities [23–26] and trainability via Variational Monte Carlo (VMC) [27], NQS performance nevertheless degrades in frustrated regimes, whether frustration is induced by competing interactions on bipartite lattices or is intrinsic to non-bipartite geometries. This degradation reflects both challenging optimization dynamics [28, 29] and poor

generalization of the GS sign structure [30]. In unfrustrated systems, MSR fixes the GS sign structure exactly; however, once it fails in frustrated Hamiltonians, the GS develops a nontrivial phase pattern whose microscopic origin remains elusive and which standard NQS often fail to reproduce [31]. We refer to this challenge, namely reconstructing the correct GS phase structure, as the Phase Reconstruction Problem (PRP).

Early work by Richter *et al.* [32] used Exact Diagonalization (ED) and spin-wave theory to determine the GS sign structure of the square-lattice  $J_1$ – $J_2$  model. Work by Westerhout *et al.* [31] proposed a reconstruction scheme by mapping GS signs to a non-glassy auxiliary Ising model defined on a subset of basis states. Recently, Boolean–Fourier methods have been applied to the frustrated HAF [33]. While these approaches expose important aspects of sign complexity, a general structural account of how geometric frustration induces *global* sign constraints remains only partially developed. Here we analyze PRP as a weighted Max-Cut (QUBO) instance on the HG and derive structural criteria for global phase/sign consistency, thereby providing a complementary structural viewpoint to Ref. [31].

**Formalism.** We represent the physical lattice as a simple, undirected, connected graph  $G = (V, E, J)$ , whose vertices  $i \in V$  carry spin- $\frac{1}{2}$  degrees of freedom  $\hat{\mathbf{S}}_i = \frac{1}{2}\hat{\boldsymbol{\sigma}}_i$ . The edge set  $E$  specifies the pairs of sites along which exchange interactions act, and  $J : E \rightarrow \mathbb{R}$  encodes their strengths.

Throughout this work we consider the  $J_1$ – $J_2$  Heisenberg model, which includes only nearest-neighbor (NN) and next-nearest-neighbor (NNN) couplings. Defining  $E_r = \{\{i, j\} : d(i, j) = r\}$  for  $r = 1, 2$ , where  $d(i, j)$  is the graph distance on  $G$ , we take  $E = E_1 \cup E_2$  and define the coupling function  $J : E \rightarrow \mathbb{R}$  by  $J(\{i, j\}) = J_1$  for  $\{i, j\} \in E_1$  and  $J(\{i, j\}) = J_2$  for  $\{i, j\} \in E_2$ .

For antiferromagnetic couplings  $J_1, J_2 > 0$ , the Hamil-

tonian is

$$\hat{H} = J_1 \sum_{\{i,j\} \in E_1} \hat{\mathbf{S}}_i \cdot \hat{\mathbf{S}}_j + J_2 \sum_{\{i,j\} \in E_2} \hat{\mathbf{S}}_i \cdot \hat{\mathbf{S}}_j. \quad (1)$$

We can split (1) into diagonal and off-diagonal parts by rewriting it as,  $\hat{H} = \sum_{r=1}^2 J_r (\hat{H}_r^{zz} + 1/2 \hat{H}_r^\pm)$ . Here, each  $\hat{H}_r^{zz} = \sum_{\{i,j\} \in E_r} \hat{S}_i^z \hat{S}_j^z$  is the Ising contribution, which is diagonal in the computational basis, and assigning a bond energy to each edge at range  $r$ . The quantum part is captured by the off-diagonal operators  $\hat{H}_r^\pm = \sum_{\{i,j\} \in E_r} \hat{S}_i^+ \hat{S}_j^- + \hat{S}_i^- \hat{S}_j^+$ , which flip a single antiparallel pair ( $\uparrow_i \downarrow_j \leftrightarrow \downarrow_i \uparrow_j$ ) at range  $r$  ( $r = 1$  for NN,  $r = 2$  for NNN), thereby acting as the edge generators of the HG.

**Heisenberg flip (HF).** We choose the computational basis diagonal in  $\hat{S}^z$  and each basis state,  $\sigma \in \{-1, +1\}^{|V|}$ . The off-diagonal operators  $\hat{H}_r^\pm$  connect two configurations only when a single antiparallel pair occurs on an interaction edge. For the  $J_1$ - $J_2$  model these interaction edges lie in  $E_1$  (NN) or  $E_2$  (NNN). Given  $\sigma$ , choose sites  $\{i,j\} \in E_1 \cup E_2$  with  $\sigma_i = -\sigma_j$ . Flipping the spins at sites  $i$  and  $j$  produces a new configuration  $\tau$ , written  $\sigma \rightarrow \tau$ , and we call this a *Heisenberg flip* (HF). We denote the sets of NN and NNN HFs by  $\mathcal{R}_1 = \{\{\sigma, \tau\} : \sigma \rightarrow \tau \text{ via } E_1\}$  and  $\mathcal{R}_2 = \{\{\sigma, \tau\} : \sigma \rightarrow \tau \text{ via } E_2\}$ , and the corresponding NN and NNN neighbors of  $\sigma$  by  $\mathcal{N}_1(\sigma) = \{\tau : \{\sigma, \tau\} \in \mathcal{R}_1\}$  and  $\mathcal{N}_2(\sigma) = \{\tau : \{\sigma, \tau\} \in \mathcal{R}_2\}$ .

**Hilbert Graph (HG).** For a given physical graph  $G$ , we define its Hilbert Graph,  $\Gamma(G) = (\mathcal{V}, \mathcal{E})$  as follows. The vertex set  $\mathcal{V} = \{-1, +1\}^{|V|}$  consists of all computational basis states and the edge set  $\mathcal{E} = \mathcal{R}_1 \cup \mathcal{R}_2$ , consists of pairs of states connected by NN or NNN HF. The HGs of the square-lattice  $J_1$ - $J_2$  model and the triangular lattice are denoted by  $\Gamma(\text{XX})$  and  $\Gamma(\text{A})$ , respectively. An illustration of  $\Gamma(\text{XX})$  for the  $2 \times 2$  square lattice in the zero-magnetization sector is shown in Fig. 1.

We note that the HG is closely related to a class of graphs known as *token graphs*  $F_k(G)$  [34], where one places  $k$  indistinguishable *tokens* on the vertices of a base graph  $G$ , and edges connect configurations that differ by moving a single token along an edge of  $G$ . In standard token graphs, the allowed moves are purely combinatorial, i.e., any token may traverse any edge. In contrast, the HG is *operator-driven*: the off-diagonal Hamiltonians  $\hat{H}_r^\pm$  define the allowable flips (NN, NNN) and serve as token generators.

**Unweighted adjacency matrix.** Edges of the HG are generated solely by the off-diagonal terms,  $\hat{H}_r^\pm$ . Thus, the connectivity of this graph is defined by the adjacency matrix,  $A_{\sigma\tau}^\Gamma = \min(1, \sum_{r=1}^2 (A_r^\Gamma)_{\sigma\tau})$ . Where,

$$(A_r^\Gamma)_{\sigma\tau} = \langle \sigma | \hat{H}_r^\pm | \tau \rangle = \begin{cases} 1, & \{\sigma, \tau\} \in \mathcal{E}_r \\ 0, & \text{otherwise} \end{cases} \quad (2)$$

$A_r^\Gamma$  represents the connectivity of the NN ( $r = 1$ ) and NNN ( $r = 2$ ) subgraphs.

**Weighted adjacency matrix.** We represent a many-body wavefunction,  $|\Psi\rangle = \sum_\sigma c_\sigma |\sigma\rangle$  in an orthonormal basis with  $c_\sigma = \psi_\sigma e^{i\phi_\sigma}$ ,  $\psi_\sigma, \phi_\sigma \in \mathbb{R}$  and  $\psi_\sigma \geq 0$ . Let  $Z = \sum_\sigma \psi_\sigma^2$  denote the normalization. Then, the amplitude-weighted adjacency matrix is defined as  $W_{\sigma\tau}^\Gamma = \sum_r (W_r^\Gamma)_{\sigma\tau}$ , where

$$(W_r^\Gamma)_{\sigma\tau} = \frac{J_r}{Z} \psi_\sigma \psi_\tau (A_r^\Gamma)_{\sigma\tau}. \quad (3)$$

The matrix elements of  $W^\Gamma$  thus acts as emergent couplings on the HG: for each bond type  $r$ , the effective coupling on an edge  $\{\sigma, \tau\} \in \mathcal{E}_r$  is  $(W_r^\Gamma)_{\sigma\tau}$ , where  $\psi_\sigma \psi_\tau$  provides the state-dependent amplitude factor. When amplitudes are nonzero, both  $A^\Gamma$  and  $W^\Gamma$  share the same sparsity pattern; only the edge weights differ, reflecting the amplitudes of the chosen state and the couplings  $J_1$  and  $J_2$ .

**Triangles in the HG.** Given the unweighted adjacency matrix  $A^\Gamma$  of an HG, the number of elementary triangles is  $N_\Delta = \frac{1}{6} \text{tr}(A^\Gamma)^3$ , so  $N_\Delta = 0$  if and only if  $\Gamma$  is triangle-free [35]. For the NN Heisenberg model on a bipartite lattice, every HF preserves sublattice parity, hence the HG is bipartite and therefore triangle-free. Adding the same-sublattice couplings (e.g.  $J_2$  on the square lattice) or starting from a non-bipartite geometry (triangular, kagome) produces triangles in the HG, introducing incompatible phase constraints around 3-cycles. This leads to the following structural fact relating the physical lattice  $G$  to its HG  $\Gamma(G)$ :

**Theorem 1 (Bipartiteness inheritance)** *Let  $G = (V_A \cup V_B, E)$  be a bipartite lattice and consider the spin- $\frac{1}{2}$  Hilbert space restricted to a fixed  $S_{\text{tot}}^z$  sector. Let  $\Gamma(G)$  be the HG whose vertices are configurations  $\sigma$  in this sector, and where  $\{\sigma, \tau\}$  is an edge if and only if  $\tau$  is obtained from  $\sigma$  by a single NN HF ( $\uparrow_i \downarrow_j \leftrightarrow \downarrow_i \uparrow_j$ ) on a bond  $(i, j) \in E$ . Then  $\Gamma(G)$  is bipartite [36].*

The converse statement also holds: non-bipartite physical lattices induce non-bipartite HGs (indeed, any odd cycle in  $G$  yields an odd cycle in  $\Gamma(G)$  in a fixed- $S_{\text{tot}}^z$  sector) [36].

**Energy.** The energy associated with a variational state can be split into two parts,  $E = E_c + E_q$ . The classical part,  $E_c = 1/Z \sum_\sigma \psi_\sigma^2 H_{\sigma\sigma} = 1/4 - 1/(2Z) \sum_\sigma \sum_{r=1}^2 J_r a_\sigma^{(r)} \psi_\sigma^2$ , where  $a_\sigma^{(r)}$  counts the number of *domain walls* (antiparallel spin pairs) at range  $r$  in configuration  $\sigma$ . It is phase independent and therefore provides a stabilizing background energy. The quantum part can be reduced to a *weighted XY* model defined on the HG, and can be written as  $E_q = \frac{1}{Z} \sum_{\sigma \neq \tau} |H_{\sigma\tau}| \psi_\sigma \psi_\tau \cos(\phi_\tau - \phi_\sigma + \theta_{\sigma\tau})$ . Since the phase  $\theta_{\sigma\tau}$  of the matrix element  $H_{\sigma\tau}$  is zero for the  $J_1$ - $J_2$  system, the energy reduces to,

$$E_q = \sum_{\{\sigma, \tau\} \in \mathcal{E}} W_{\sigma\tau}^\Gamma \cos(\phi_\sigma - \phi_\tau) \quad (4)$$

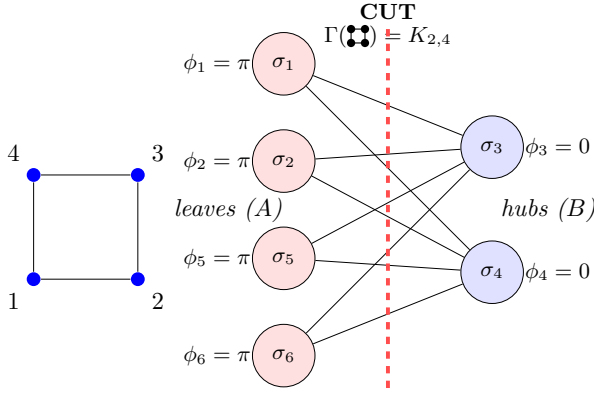


FIG. 1: **Left:** A  $2 \times 2$  open boundary square-lattice Heisenberg antiferromagnet with sites labeled by integers. **Right:** Corresponding bipartite HG  $K_{2,4}$  in the  $S_{\text{total}}^z = 0$  sector, with hub vertices  $\{\sigma_3, \sigma_4\}$  corresponding to Néel configurations (blue) and leaf vertices  $\{\sigma_1, \sigma_2, \sigma_5, \sigma_6\}$  corresponding to non-Néel configurations (purple). With phases  $\phi_{3,4} = 0$  and  $\phi_{1,2,5,6} = \pi$ , every NN edge crosses the Max-Cut, yielding the antiferromagnetic energy minimum. The states  $\sigma_i$  are labeled such that,  $\sigma_1 = \uparrow_1 \uparrow_2 \downarrow_3 \downarrow_4$ ,  $\sigma_2 = \downarrow_1 \downarrow_2 \uparrow_3 \uparrow_4$ ,  $\sigma_5 = \uparrow_1 \downarrow_2 \downarrow_3 \uparrow_4$ ,  $\sigma_6 = \downarrow_1 \uparrow_2 \uparrow_3 \downarrow_4$  and  $\sigma_3 = \uparrow_1 \downarrow_2 \uparrow_3 \downarrow_4$ ,  $\sigma_4 = \downarrow_1 \uparrow_2 \downarrow_3 \uparrow_4$ .

This graph-theoretic formulation using the weight matrix makes explicit that when amplitudes are frozen, the genuinely quantum content of the variational problem resides in the *phase differences along the edges*: the amplitudes determine the interaction strengths (edge weights), while the phases control constructive or destructive interference through the factor  $\cos(\phi_\sigma - \phi_\tau)$ .

**Continuous phase optimization.** For continuous phase variables  $\{\phi_\sigma\}$  and fixed amplitudes  $\{\psi_\sigma\}$ , the phase-dependent part of the variational energy (4) can be recast by expressing each phase as a unit vector  $u_\sigma = (\cos \phi_\sigma, \sin \phi_\sigma) \in \mathbb{R}^2$ . Collecting the cosine and sine components into the column vectors  $c = (\cos \phi_1, \dots, \cos \phi_n)^\top$  and  $s = (\sin \phi_1, \dots, \sin \phi_n)^\top$ , the phase field becomes the matrix  $U = [c \ s] \in \mathbb{R}^{n \times 2}$ . With this representation, (4) takes the Laplacian form

$$E_q(\Gamma) = E_0 - \frac{1}{2} \sum_{\{\sigma, \tau\} \in \mathcal{E}} W_{\sigma\tau}^\Gamma \|u_\sigma - u_\tau\|^2, \quad (5)$$

where  $E_0 = \sum_{\{\sigma, \tau\} \in \mathcal{E}} W_{\sigma\tau}^\Gamma$  is independent of the phases. Here  $\|u_\sigma - u_\tau\|^2 = 2[1 - \cos(\phi_\sigma - \phi_\tau)]$ , and the quadratic form in (5) is the Dirichlet energy associated with the amplitude-weighted graph Laplacian of the HG.

Minimizing  $E_q$  under the nonlinear constraints  $\|u_\sigma\| = 1$  for all vertices yields the Karush–Kuhn–Tucker

(KKT) [36–38] stationery conditions

$$\sum_{\tau \in \mathcal{N}(\sigma)} W_{\sigma\tau}^\Gamma \sin(\phi_\sigma - \phi_\tau) = 0, \quad \forall \sigma, \quad (6)$$

The solutions of these equations correspond to zero gradients of  $E_q$  with respect to  $\phi_\sigma$ . The discrete phase assignment  $\phi_\sigma \in \{0, \pi\}$  (modulo  $2\pi$ ) is an obvious solution of the stationarity equations. For  $n$  states, there are  $2^n$  such discrete phase assignments. Whenever a variational ansatz can realize such an assignment, these solutions also correspond to zero gradients of  $E_q$  with respect to the variational parameters of the ansatz, by the chain rule. Moreover, if  $\{\phi_\sigma\}$  is a solution, then  $\{\phi_\sigma + \delta\}$  is also a solution for any constant  $\delta$ , as a direct consequence of the global phase symmetry. Modulo this global shift symmetry, the  $\{0, \pi\}$  assignments organize into  $2^{n-1}$  distinct one-parameter families (“lines”) in the phase space (modulo  $2\pi$ ) that correspond to stationary points of  $E_q$ . If a stationary point does not minimize or maximize  $E_q$  globally, then it corresponds to a saddle point as shown by Burer *et al.* [39]. Even so, the exponential scaling of the number of such stationary manifolds suggests increasing difficulty in navigating the phase landscape for larger lattice sizes using variational optimization.

**Discrete phase optimization.** Following the continuous-phase relaxation, the invariance of the  $J_1$ – $J_2$  Hamiltonian under complex conjugation implies that a GS can be chosen with real coefficients. Under this restriction, and for the antiferromagnetic spin-flip matrix elements in Eq. (4), each HG edge is locally optimized when the phase difference across it equals  $\pi$ , which we refer to as the  $\pi$ -edge condition (PEC):

$$\phi_\sigma - \phi_\tau \equiv \pi \pmod{2\pi} \quad \text{for all } (\sigma, \tau) \in \Gamma(G). \quad (7)$$

Since PEC imposes locally optimal destructive interference on every edge, whether this condition can be satisfied globally depends entirely on the structure of the HG. This structural observation leads to the following theorem:

**Theorem 2 (PEC-bipartiteness)** *A global  $\{0, \pi\}$  phase assignment obeying PEC on every active edge exists if and only if  $\Gamma(G)$  is bipartite [36].*

In a bipartite HG, the two partitions can be assigned phases  $\{0, \pi\}$  so that every edge satisfies PEC simultaneously. If the HG contains an odd cycle, at least one edge must necessarily violate PEC. Thus, triangles on the HG are the elementary obstruction to a global PEC assignment, making them the microscopic carriers of geometric frustration in the HG. Removing zero-weight edges or restricting to a fixed  $S^z$  sector (an induced subgraph) preserves bipartiteness and therefore the equivalence. Moreover, a global PEC assignment remains exact when the NN couplings are antiferromagnetic, and the NNN couplings are ferromagnetic [36].

**PEC & MSR.** For a bipartite physical lattice  $G$ , HFs connect states  $(\sigma, \tau) \in \Gamma(G)$  whose number of up-spins on a particular sublattice ( $A$ ) differs by one. Define  $N_A^\uparrow(\sigma) := \sum_{i \in A} (1 + \sigma_i)/2$  and  $\phi_\sigma := \pi N_A^\uparrow(\sigma)$ , so that Eq. (7) holds. In other words, PEC is globally satisfied, and the wavefunction acquires the Marshall phase  $c_\sigma = (-1)^{N_A^\uparrow(\sigma)} \psi_\sigma$  [8], making the GS Marshall-positive up to a global phase. Thus, global PEC on  $\Gamma(G)$  reproduces the Marshall sign structure of unfrustrated Heisenberg anti-ferromagnets: MSR appears as the unique global phase field compatible with enforcing  $\phi_\sigma - \phi_\tau = \pi$  on every edge. Its breakdown signals the onset of frustration. We emphasize that Marshall's original proof [8] proceeds by contradiction and does *not* use the graph-theoretical viewpoint adopted in this work [36].

**PEC &  $\mathbb{Z}_2$  grading.** The HG  $\Gamma(G)$  of the bipartite HAF admits a natural  $\mathbb{Z}_2$  structure on its vertices, and once the PEC fixes the Marshall phase field, this structure becomes visible at the level of wavefunctions. The associated gauge transformation is generated by the unitary involution

$$\hat{\eta}_A := (-1)^{\hat{N}_A^\uparrow} = \prod_{i \in A} \hat{\sigma}_i^z, \quad (8)$$

where  $\hat{N}_A^\uparrow = \sum_{i \in A} \frac{1}{2}(\mathbb{1} + \hat{\sigma}_i^z)$  counts up-spins on the  $A$  sublattice. The operator  $\hat{\eta}_A$  is the Lieb–Mattis operator [40, 41]; expressing it in the form (8) makes its role as a graph-partition operator on  $\Gamma(G)$  explicit, implementing the  $\mathbb{Z}_2$  two-coloring of the HG. This reveals a global  $\mathbb{Z}_2$  symmetry generated by  $\hat{\eta}_A$ , analogous to the fermionic parity operator  $(-1)^F$  in supersymmetric quantum mechanics [42]. On basis configurations,  $\hat{\eta}_A|\sigma\rangle = (-1)^{N_A^\uparrow(\sigma)}|\sigma\rangle$ , with  $(-1)^{N_A^\uparrow(\sigma)} = \pm 1$  for even/odd  $N_A^\uparrow(\sigma)$ . This eigenvalue labels each vertex of  $\Gamma(G)$  and induces the  $\mathbb{Z}_2$  bipartition  $\mathcal{V} = \mathcal{V}_+ \sqcup \mathcal{V}_-$ , where  $\mathcal{V}_\pm = \{\sigma : (-1)^{N_A^\uparrow(\sigma)} = \pm 1\}$ .

The involution  $\hat{\eta}_A$  acts as a *cut* operator: its existence is equivalent to the  $\mathbb{Z}_2$  bipartition of  $\Gamma(G)$ , and the parity eigenvalues  $\pm 1$  label the two sides of this cut. Every NN HF changes  $N_A^\uparrow$  by  $\pm 1$  and must cross the cut, so all off-diagonal Hamiltonian matrix elements share the same sign in this gauge, producing a stoquastic representation. As shown in Fig. 1, this cut fixes the gauge that minimizes the off-diagonal contribution  $E_q$ , linking the bipartition to energy minimization. As a byproduct, the Lieb–Mattis involution also implies a sublattice-parity selection rule for  $\langle \hat{\eta}_A \rangle$  (in particular,  $\langle \hat{\eta}_A \rangle = 0$  for  $N = 4L + 2$  in  $S_{\text{tot}}^z = 0$  when a sublattice-exchanging symmetry exists; see [36]).

Beyond the bipartite case,  $\Gamma(G)$  is not two-colorable, and the PEC cannot be satisfied globally, so the phase-dependent energy  $E_q$  becomes a genuine combinatorial optimization problem on  $\Gamma(G)$ . We therefore turn to its worst-case computational complexity by rewriting  $E_q$  as a quadratic binary objective.

**Equivalence to weighted Max-Cut.** We now identify the complexity class underlying the discrete phase optimization problem in Eq. (4). Introduce Ising variables  $s_\sigma \in \{\pm 1\}$  and encode  $\mathbb{Z}_2$  phases by  $\phi_\sigma = \frac{\pi}{2}(1 - s_\sigma)$ , so that  $\cos(\phi_\sigma - \phi_\tau) = s_\sigma s_\tau$ . Then Eq. (4) reduces to the quadratic binary objective reduces to

$$E_q(\Gamma) = \sum_{\{\sigma, \tau\} \in \mathcal{E}} W_{\sigma\tau}^\Gamma s_\sigma s_\tau, \quad W_{\sigma\tau}^\Gamma \geq 0. \quad (9)$$

i.e. a QUBO [43] instance on the HG  $\Gamma(G)$ . We note that Ref. [31] studies the practical optimization of an induced auxiliary Ising objective of the form of Eq. (9) via simulated annealing and a deterministic greedy heuristic, but does not conduct a worst-case computational complexity analysis.

Any assignment  $\{s_\sigma\}$  defines a cut  $(\mathcal{V}_+, \mathcal{V}_-)$  of  $\Gamma(G)$  by  $\mathcal{S}_\pm = \{\sigma : s_\sigma = \pm 1\}$ . For an edge  $\{\sigma, \tau\}$ , the contribution to Eq. (9) is  $-W_{\sigma\tau}^\Gamma$  if  $\sigma$  and  $\tau$  lie on opposite sides of the cut ( $s_\sigma s_\tau = -1$ ), and  $+W_{\sigma\tau}^\Gamma$  if they lie on the same side ( $s_\sigma s_\tau = +1$ ). Writing  $1_{\text{cut}}(\sigma, \tau) = \frac{1-s_\sigma s_\tau}{2}$ , we obtain

$$E_q(\Gamma) = \sum_{\{\sigma, \tau\} \in \mathcal{E}} W_{\sigma\tau}^\Gamma - 2 \sum_{\{\sigma, \tau\} \in \text{cut}} W_{\sigma\tau}^\Gamma. \quad (10)$$

Since the first term is constant, minimizing  $E_q(\Gamma)$  is equivalent to maximizing the cut weight  $\sum_{\{\sigma, \tau\} \in \text{cut}} W_{\sigma\tau}^\Gamma$ , i.e. the *weighted Max-Cut* problem on  $\Gamma(G)$  with edge weights  $W_{\sigma\tau}^\Gamma$ . Consequently, in the worst case over  $\Gamma(G)$  instances, discrete PRP is NP-hard [44]. This difficulty is distinct from the quantum Monte Carlo sign problem [45]: here the obstruction arises from an NP-hard combinatorial optimization over  $\{s_\sigma\}$ , not from sampling oscillatory path-integral weights.

**SDP relaxation & GW approximation.** Although weighted Max-Cut is NP-hard, it admits efficient approximation algorithms. A trivial baseline is a uniformly random assignment  $s_\sigma \in \{\pm 1\}$ , which for nonnegative edge weights yields an expected cut weight equal to one half of the total edge weight (a universal  $\frac{1}{2}$ -approximation).

A stronger guarantee follows from a semidefinite programming (SDP) relaxation [46]. In the SDP, each binary variable  $s_\sigma$  is relaxed to a unit vector  $\mathbf{v}_\sigma$  (equivalently, to a positive-semidefinite Gram matrix), and the discrete products  $s_\sigma s_\tau$  are replaced by inner products  $\mathbf{v}_\sigma \cdot \mathbf{v}_\tau$ . The Goemans–Williamson (GW) algorithm [47] solves this relaxation and then applies randomized hyperplane rounding to recover a binary cut. For weighted Max-Cut, it achieves an expected approximation ratio of at least 0.878 of the optimum, which is the best known worst-case guarantee among polynomial-time algorithms under standard complexity assumptions [36, 47].

In practice, however, the SDP underlying the GW relaxation scales poorly with HG size, limiting its direct applicability to small systems. Throughout this work, GW therefore serves primarily as a conceptual benchmark for

phase optimization rather than as a scalable computational tool. Motivated by this scalability limitation, the unit-circle relaxation discussed above can be viewed as a rank-two restriction of the SDP variable, yielding a *nonconvex* but computationally cheaper alternative to the full SDP. Closely related rank-two relaxations and heuristics have been explored in the optimization literature [39]. The key trade-off is that this low-rank restriction destroys convexity, so one should not expect certificates or global optimality guarantees in general, nor an escape from worst-case computational hardness.

**VMC & Max-Cut.** The graph-theoretic formulation clarifies the distinct roles of amplitudes and phases in variational wavefunction optimization, and highlights the additional structural difficulty posed by phase degrees of freedom.

Starting from the amplitude–phase decomposition  $\Psi_\theta(\sigma) = \psi_\theta(\sigma)e^{i\phi_\theta(\sigma)}$  and restricting the phases to the  $\mathbb{Z}_2$  manifold  $\phi_\theta(\sigma) \in \{0, \pi\}$ , we introduce sign variables  $s_\sigma := \cos \phi_\theta(\sigma) \in \{\pm 1\}$ , so that  $\cos[\phi_\theta(\sigma) - \phi_\theta(\tau)] = s_\sigma s_\tau$ . Defining the amplitude ratio  $\rho_{\sigma\tau}(\theta) := \psi_\theta(\tau)/\psi_\theta(\sigma)$ , the phase-dependent contribution of energy becomes the quadratic form  $E_\phi[s] = \sum_\sigma \Pi_\theta(\sigma) \sum_\tau H_{\sigma\tau}^\pm \rho_{\sigma\tau}(\theta) s_\sigma s_\tau$ . For the  $J_1$ – $J_2$  model the off-diagonal elements decompose as  $H_{\sigma\tau}^\pm = J_1 K_{\sigma\tau}^{(1)} + J_2 K_{\sigma\tau}^{(2)}$ . Introducing  $C_{\sigma\tau}^{(r)} := \Pi_\theta(\sigma) K_{\sigma\tau}^{(r)} \rho_{\sigma\tau}(\theta)$ ,  $r = 1, 2$ , and symmetrising,  $J_{\sigma\tau}^{(r)}(\theta) := \frac{1}{2}(C_{\sigma\tau}^{(r)} + C_{\tau\sigma}^{(r)})$ , we obtain the effective interaction  $\tilde{J}_{\sigma\tau}(\theta; J_1, J_2) := J_1 J_{\sigma\tau}^{(1)}(\theta) + J_2 J_{\sigma\tau}^{(2)}(\theta)$ , which combines all NN and NNN spin-flip edges of the HG and yields

$$E_\phi[s; \theta] = \sum_{\sigma < \tau} \tilde{J}_{\sigma\tau}(\theta; J_1, J_2) s_\sigma s_\tau. \quad (11)$$

Eq. (11) makes the separation between amplitude and phase optimization explicit. The amplitudes  $\psi_\theta(\sigma) \geq 0$  enter through the sampling weights  $\Pi_\theta(\sigma)$  and local amplitude ratios  $\rho_{\sigma\tau}(\theta) = \psi_\theta(\tau)/\psi_\theta(\sigma)$ , which are learned by standard VMC updates over a smooth parameter space. In contrast, once phases are restricted to  $\mathbb{Z}_2$  values, the remaining dependence on  $\phi_\theta$  is encoded entirely in binary variables  $s_\sigma \in \{\pm 1\}$  and their induced couplings  $\tilde{J}_{\sigma\tau}(\theta; J_1, J_2)$ . Thus, for (approximately) fixed amplitudes, phase optimization reduces to an Ising/QUBO problem on the HG with couplings  $\tilde{J}_{\sigma\tau}(\theta; J_1, J_2)$ , Eq. (11). When  $\tilde{J}_{\sigma\tau} \geq 0$ , this objective is equivalent (up to an additive constant) to weighted Max-Cut via Eq. (10).

The Max-Cut viewpoint makes the PEC’s role transparent. For  $\tilde{J}_{\sigma\tau} \geq 0$ , each active edge  $\{\sigma, \tau\}$  (i.e.,  $\tilde{J}_{\sigma\tau} > 0$ ) is locally minimized by a  $\pi$  phase difference, equivalently  $s_\sigma s_\tau = -1$ . Hence, satisfying the PEC on all active edges is exactly the existence of a global  $\mathbb{Z}_2$  assignment  $\{s_\sigma = \pm 1\}$  that two-colors the active-edge subgraph of  $\Gamma(G)$  (i.e., that subgraph is bipartite). When

such an assignment exists, every active edge is simultaneously satisfied, and the phase-dependent objective is saturated, giving

$$E_\phi[s; \theta] = - \sum_{\sigma < \tau} \tilde{J}_{\sigma\tau}(\theta; J_1, J_2)$$

(up to the constant shift in Eq. (10)). In this case, there is no residual discrete sign learning: VMC updates need only learn the smooth amplitudes  $\psi_\theta(\sigma)$ .

When a global PEC assignment does *not* exist, the active-edge subgraph of  $\Gamma(G)$  is non-bipartite and contains odd cycles. Then the local  $\pi$  preferences on edges are mutually incompatible: any choice of  $\{s_\sigma\}$  leaves a frustrated subset of edges with  $s_\sigma s_\tau = +1$ . In Max-Cut language, the optimum cut fails to include all active edges, and the residual phase energy is set by the *minimum* total weight of unsatisfied edges (equivalently, the *maximum* total weight of satisfied ones). Consequently, even for (approximately) fixed amplitudes, phase optimization remains a genuinely *global* combinatorial problem on  $\Gamma(G)$ : changing a sign on a single vertex flips the satisfaction status of all incident edges, so the best assignment is determined by the global pattern of frustration rather than local consistency. In the variational setting, the couplings  $\tilde{J}_{\sigma\tau}(\theta; J_1, J_2)$  are themselves induced by the current amplitudes, so amplitude learning and sign learning become coupled: VMC updates that improve  $\psi_\theta$  also reshapes the effective Ising/QUBO instance, while the optimizer must simultaneously seek a near-optimal cut (sign pattern) for the evolving weighted graph.

If a variational family with no explicit phase prior nonetheless reaches GS with high accuracy, this indicates that it has implicitly learned an *energetically effective* sign structure on the induced HG. In the language of this work, the ansatz has found a high-quality cut for the induced weighted Max-Cut/QUBO objective, reproducing the GS sign pattern on the configurations that dominate the variational energy. A detailed numerical study of the associated computational complexity on  $\Gamma(G)$  will be presented in forthcoming work.

**Acknowledgement.** We are grateful to Zohar Nussinov, David A. Huse, Ruy Fabila, Ernesto Estrada, Sam Hopkins, and Filippo Vicentini for their insightful discussions and comments. We also extend our sincere thanks to Georg Schwiete and Nobuchika Okada for their careful reading of the manuscript and their valuable suggestions. MAS and PTA are grateful to the National Science Foundation (NSF) for financial support under Grant No. [1848418]. M.H acknowledges support from the Natural Sciences and Engineering Research Council of Canada (NSERC).

---

\* mashamim@crimson.ua.edu  
 † moshiur\_rahman@utanota.com  
 ‡ mhibatallah@uwaterloo.ca  
 § ptaraujo@ua.edu

[1] C. K. Majumdar and D. K. Ghosh, *Journal of Mathematical Physics* **10**, 1388 (1969).

[2] C. K. Majumdar and D. K. Ghosh, *Journal of Mathematical Physics* **10**, 1399 (1969).

[3] B. S. Shastry and B. Sutherland, *Physica B+C* **108**, 1069 (1981).

[4] U. Schollwöck, *Ann. Phys.* **326**, 96 (2011).

[5] R. Orús, *Ann. Phys.* **349**, 117 (2014).

[6] F. Becca, L. Capriotti, A. Parola, and S. Sorella, arXiv e-prints , arXiv:0905.4854 (2009), arXiv:0905.4854 [cond-mat.str-el].

[7] G. Carleo and M. Troyer, *Science* **355**, 602 (2017), arXiv:1606.02318 [cond-mat.dis-nn].

[8] W. Marshall, *Proceedings of the Royal Society of London. Series A. Mathematical and Physical Sciences* **232**, 48 (1955).

[9] M. Hibat-Allah, M. Ganahl, L. E. Hayward, R. G. Melko, and J. Carrasquilla, *Physical Review Research* **2**, 023358 (2020), arXiv:2002.02973 [cond-mat.dis-nn].

[10] M. S. Moss, R. Wiersema, M. Hibat-Allah, J. Carrasquilla, and R. G. Melko, *Phys. Rev. B* **112**, 134449 (2025), arXiv:2505.20406 [cond-mat.str-el].

[11] C. Roth, arXiv e-prints , arXiv:2003.06228 (2020), arXiv:2003.06228 [physics.comp-ph].

[12] K. Choo, T. Neupert, and G. Carleo, *Phys. Rev. B* **100**, 125124 (2019), arXiv:1903.06713 [cond-mat.str-el].

[13] A. Chen, K. Choo, N. Astrakhantsev, and T. Neupert, *Physical Review Research* **4**, L022026 (2022), arXiv:2111.06411 [cond-mat.str-el].

[14] C. Roth and A. H. MacDonald, arXiv e-prints , arXiv:2104.05085 (2021), arXiv:2104.05085 [quant-ph].

[15] X. Liang, W.-Y. Liu, P.-Z. Lin, G.-C. Guo, Y.-S. Zhang, and L. He, *Phys. Rev. B* **98**, 104426 (2018), arXiv:1807.09422 [cond-mat.str-el].

[16] M. A. Shamim, E. A. F. Reinhardt, T. A. Chowdhury, S. Gleyzer, and P. T. Araujo, *Phys. Rev. B* **113**, 045157 (2026).

[17] F. Ferrari, F. Becca, and J. Carrasquilla, *Physical Review B* **100**, 125131 (2019).

[18] Y. Nomura, A. S. Darmawan, Y. Yamaji, and M. Imada, *Phys. Rev. B* **96**, 205152 (2017), arXiv:1709.06475 [cond-mat.str-el].

[19] L. L. Viteritti, R. Rende, and F. Becca, *Phys. Rev. Lett.* **130**, 236401 (2023), arXiv:2211.05504 [cond-mat.dis-nn].

[20] L. Loris Viteritti, R. Rende, A. Parola, S. Goldt, and F. Becca, arXiv e-prints , arXiv:2311.16889 (2023), arXiv:2311.16889 [cond-mat.str-el].

[21] R. Rende, L. Loris Viteritti, L. Bardone, F. Becca, and S. Goldt, arXiv e-prints , arXiv:2310.05715 (2023), arXiv:2310.05715 [cond-mat.str-el].

[22] R. Rende, L. Loris Viteritti, F. Becca, A. Scardicchio, A. Laio, and G. Carleo, arXiv e-prints , arXiv:2502.09488 (2025), arXiv:2502.09488 [quant-ph].

[23] D.-L. Deng, X. Li, and S. Das Sarma, *Physical Review X* **7**, 021021 (2017).

[24] X. Gao and L. Duan, *Nature Communications* **8**, 662 (2017).

[25] G. Cybenko, *Mathematics of Control, Signals and Systems* **2**, 303 (1989).

[26] K. Hornik, *Neural Networks* **4**, 251 (1991).

[27] F. Becca and S. Sorella, *Quantum Monte Carlo Approaches for Correlated Systems* (Cambridge University Press, 2017).

[28] A. Szabó and C. Castelnovo, *Physical Review Research* **2**, 033075 (2020), arXiv:2002.04613 [cond-mat.str-el].

[29] M. Bukov, M. Schmitt, and M. Dupont, *SciPost Physics* **10**, 147 (2021), arXiv:2011.11214 [physics.comp-ph].

[30] T. Westerhout, N. Astrakhantsev, K. S. Tikhonov, M. Katsnelson, and A. A. Bagrov, arXiv e-prints , arXiv:1907.08186 (2019), arXiv:1907.08186 [cond-mat.dis-nn].

[31] T. Westerhout, N. Astrakhantsev, K. S. Tikhonov, M. I. Katsnelson, and A. A. Bagrov, *Nature Commun.* **11**, 1593 (2020), arXiv:1907.08186 [cond-mat.dis-nn].

[32] J. Richter, N. B. Ivanov, and K. Retzlaff, *EPL (Euro-physics Letters)* **25**, 545 (1994), arXiv:cond-mat/9407041 [cond-mat].

[33] I. Schurov, A. Kravchenko, M. I. Katsnelson, A. A. Bagrov, and T. Westerhout, arXiv preprint arXiv:2508.09870 (2025).

[34] R. Fabila-Monroy, D. Flores-Péñaloza, C. Huemer, F. Hurtado, J. Urrutia, and D. R. Wood, *Graphs and Combinatorics* **28**, 365 (2012).

[35] D. B. West, *Introduction to Graph Theory*, 2nd ed. (Prentice Hall, Upper Saddle River, NJ, 2001).

[36] M. A. Shamim, M. Rahman, M. Hibat-Allah, and P. T. Araujo, Supplementary material for: Graph-theoretic analysis of phase optimization complexity in variational wave functions for heisenberg antiferromagnets (2026), supplementary material.

[37] W. Karush, *Minima of functions of several variables with inequalities as side conditions*, Master's thesis, Department of Mathematics, University of Chicago, Chicago, Illinois (1939).

[38] H. W. Kuhn and A. W. Tucker, in *Proceedings of the Second Berkeley Symposium on Mathematical Statistics and Probability* (University of California Press, 1951) pp. 481–492.

[39] S. Burer, R. D. Monteiro, and Y. Zhang, *SIAM Journal on Optimization* **12**, 503 (2002).

[40] E. Lieb and D. Mattis, *Journal of Mathematical Physics* **3**, 749 (1962).

[41] E. Lieb and D. Mattis, *Journal of Mathematical Physics* **3**, 749 (1962).

[42] E. Witten, *Journal of Differential Geometry* **17**, 661 (1982).

[43] A. Lucas, *Frontiers in Physics* **2**, 5 (2014).

[44] R. M. Karp, in *Complexity of Computer Computations* (Plenum Press, New York, 1972) pp. 85–103.

[45] M. Troyer and U.-J. Wiese, *Phys. Rev. Lett.* **94**, 170201 (2005), arXiv:cond-mat/0408370.

[46] S. Boyd and L. Vandenberghe, *Convex Optimization* (Cambridge University Press, 2004).

[47] M. X. Goemans and D. P. Williamson, *Journal of the ACM (JACM)* **42**, 1115 (1995).